Experimental Demonstration of T:(G:G:G:G):T Hexad and T:A:A:T Tetrad Alignments within a DNA Quadruplex Stem

Mateus Webba da Silva*

Department of Medicine, Duke University Medical Center, Durham, North Carolina 27710, and Cellular Biochemistry and Biophysics Program, Memorial Sloan-Kettering Cancer Center, 1275 York Avenue, New York, New York 10021

Received October 11, 2004; Revised Manuscript Received November 29, 2004

ABSTRACT: A template-based approach was used to design unprecedented architectural motifs into a known DNA framework. The structure formed by the sequence d(GCGGTTGGAT) in 0.1 M Na^+ solution has been determined using molecular dynamics simulations constrained by distance and dihedral restraints derived from NMR experiments. The molecular topology has been previously observed for the sequence d(GCGGTGGAT) (Webba da Silva, M. (2003) *Biochemistry 42,* 14356−65). Insertion of a single thymine into the double chain reversal formed by the segment GGTGG results in the unprecedented experimental demonstration of a T:(G:G:G:G):T hexad. The bi-stranded hexad results from the pairing alignment of two G(T−G) triads. Each triad results from recognition of the sheared edge of a guanine by the Watson−Crick edge of a thymine of the segment GGTTGG. The alignment is stabilized by base-stacking of the thymine to the sugar pucker of the preceding thymine. The latter is involved in formation of the T:A:A:T tetrad alignment by forming a hydrogen bond with the free amino proton of a Watson−Crick aligned A:A mispair. We have thus established that residues in double chain reversal loops linking juxtaposed tetrads of a quadruplex stem may facilitate formation of yet unknown hydrogen bond alignments. By employing a systematic approach analysis of sequence motifs appearing in double chain reversals, bridging tetrad layers should allow for the prediction of topologies and architectural motifs appearing in biologically relevant genomic regions.

Control of the structure of matter on the molecular scale, in nature or nonbiological systems, requires the successful modulation of an array of architectural motifs based on inter- and/or intramolecular interactions. This has relevance in the discovery of principles for the design of new materials as well as uncovering the nature and stability of biologically relevant structural motifs. Some important genomic regions such as the immunoglobin switch region, telomeres, and some gene-promoter regions are believed to have the propensity to fold into DNA higher order architectures such as triplexes and quadruplexes. The formation of these architectures is affected by a variety of factors that depend primarily on hydrogen bond complementarity of bases, metal ion coordination, and equilibria but also on the nature of flanking sequences, the transcriptional activity of the region, the rate of replication through it, and the absence or presence of cofactors such as polyamines, crowding, and DNA packaging effects. In quadruplexes, the folding topologies are critically dependent on the type of loops and turns linking individual strands forming part of the stem structure. The type of loop is defined, among other factors, by how many pseudo-planar elements (layers) it spans, the number and nature of its residues, and the residue sequential context. These matters are interdependent with the glycosidic bond angle of the bases forming the tetrads in the quadruplex stem. Accordingly, the distribution of syn/anti glycosidic bond angles for (G:G:G:G) tetrads is dependent on the strand directionalities defining the stem of the topology. Thus, (anti):(syn):(anti):(syn) is characterized by adjacent antiparallel strands (*1*), (anti):(anti):(syn):(syn) appears when each strand has both a parallel and an antiparallel neighbor (*2*), and all-anti is usually characteristic of alignment of parallel stranded quadruplexes (*3*). Because of loop versatility, the G-tetrad motif has served as the basis for the development of a variety of pseudo-planar elements that includes pentads (*4*), hexads (*5*), and heptads (*6*) within quadruplex topologies. These motifs result from double chain reversals bridging contiguous tetrads spanning GGAGG segments. In them, the Hoogsteen edge of the adenine recognizes the sheared edge of a guanine of the quadruplex stem resulting in a single stranded G(A−G) triad bearing a typical A(anti) glycosidic bond angle.

Since the identification of new pairing alignments generally involves screening a large number of sequences, here we have used a template-based approach to design novel architectural elements into an existing DNA framework. We describe the structure formed by the sequence d(GCGGTTGGAT) in 0.1 M NaCl. Its molecular topology, pictured schematically in Figure 1a, has been first described for the related sequence d(GCGGTGGAT) in the same solution conditions (*7*) (Figure 1b). However, in contrast to looping thymines in GGTGG segments, the current structure exhibits both unprecedented T:(G:G:G:G):T hexad and T:A:A:T tetrad hydrogen bond alignments resultant from double chain reversals spanning contiguous tetrads in GGTTGG segments. These are shown schematically in Figure 1d,f. The stabiliza-

* To whom correspondence should addressed. Phone: (919) 681-2243; Fax: (919) 668-3925. E-mail: mateus@webbas.org.

10.1021/bi0478190 CCC: $30.25
Published on Web 02/10/2005

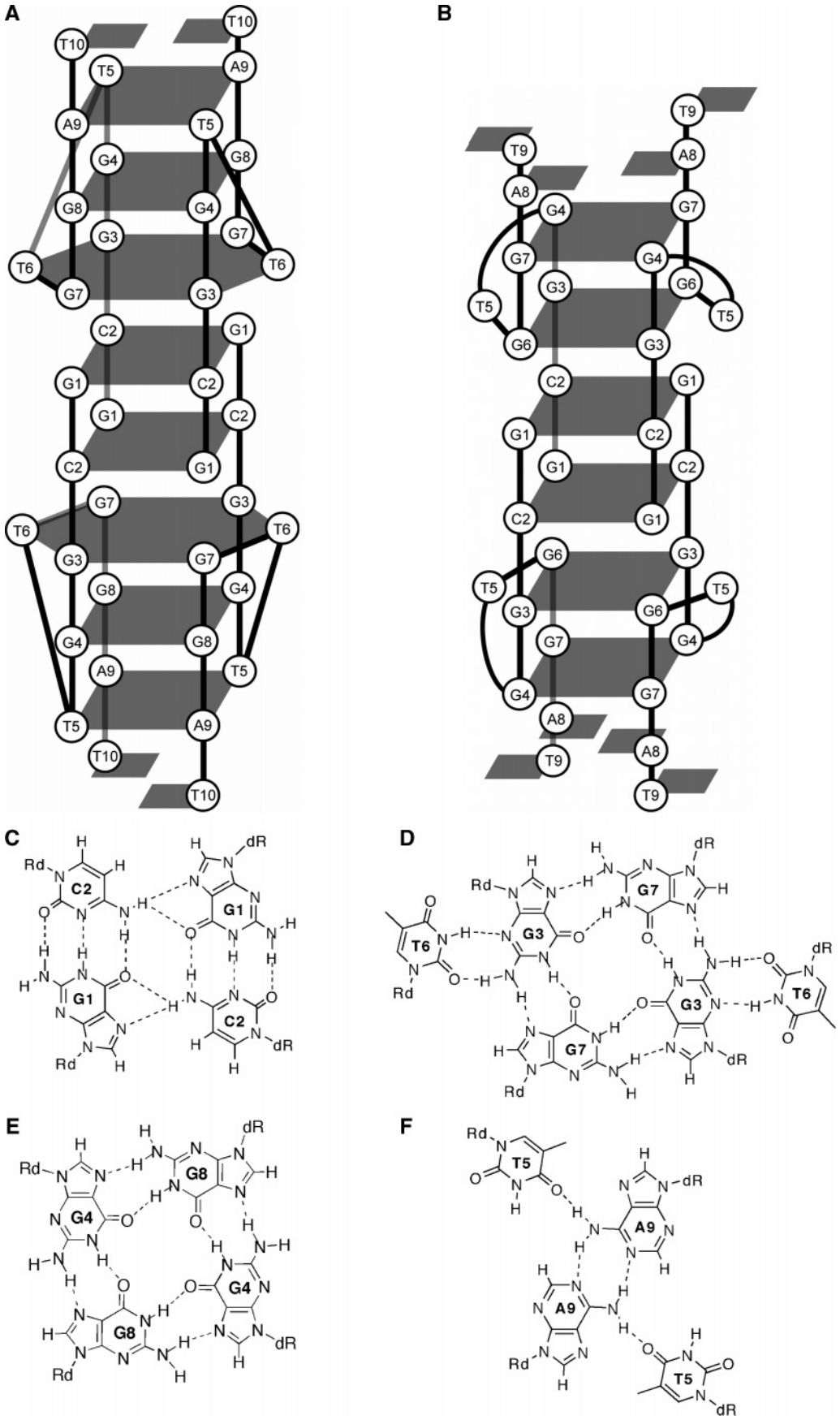

FIGURE 1: Scheme of the folding topology of the four-stranded bimolecular quadruplex formed by the sequence d(GCGGTTGGAT) (a) and d(GCGGTGGAT) (b) in 0.1 M NaCl at pH 6.8. The backbone tracing of the individual strands is shown by thick lines. All the quadruplex-stem bases adopt anti alignments in both topologies. Hydrogen bond pairing alignments for the pseudo-planar elements formed by the sequence d(GCGGTTGGAT) are depicted: (c) the four-stranded G1:C2:G1:C2 tetrad, (d) the two-stranded T6:(G3:G7:G3:G7):T6 hexad, (e) the two-stranded T5:A9:A9:T9 tetrad (d), and (e) the T10/T10 platform.

tion of looping residues in both GGTGG and GGTTGG provides insights into the formation and stabilization of double chain reversals in quadruplexes. The systematic approach thus permits the identification of structural principles that are associated with a rational based design of DNA topologies and architectural motifs. Such principles are fundamental to the prediction of topologies present in biologically significant regions. For instance, they may serve as the basis for predicting genetic instability (*8*) and consequently open possibilities for therapeutic intervention.

MATERIALS AND METHODS

Synthesis and Purification of Oligonucleotide Sequences. The nucleoside phosphoramidites and universal support CPG (controlled pore glass) were purchased from Glen Research (Sterling, VA). The nonlabeled oligonucleotide d(GCGGTTGGAT) was synthesized on a 10 μM scale on an Applied Biosystems model 392 RNA/DNA synthesizer in a DMT-ON cycle using solid phase β-cyanoethyl phosphoramidite solid-phase chemistry. The 5′-dimethoxytrityl (DMT) oligonucleotides were cleaved from the solid support, and the base-protecting groups were removed using concentrated ammonium hydroxide for 16 h at 55 °C. The full-length 5′-DMT-protected oligonucleotide was separated from failure sequences by reverse-phase high performance liquid chromatography (HPLC) on a C4 column (Rainin Instrument Co.) using a linear gradient of 2%/min of acetonitrile in 10 mM triethylammonium acetate (pH 6.8). The product was frozen at −80 °C, and the acetonitrile evaporated under vacuum. The 5′DMT group was then removed following treatment with 80% (v/v) acetic acid for 30 min. The detritylated products were extracted from the aqueous phase after addition of diethyl ether and chromatographed a second time with a linear gradient of 5%/min. The eluent containing the pure oligonucleotide was lyophilized and subsequently dialyzed several times alternatively against water and 100 mM NaCl and 2 mM sodium phosphate (pH 6.7). Two samples with uracil for thymine substitutions were also prepared. For each, a thymine of the GGTTGG segment was substituted with uracil resulting in the sequences 5′-GCGGUTGGAT-3′ and 5′-GCGGTUGGAT-3′. For these two samples, the cleavage from the solid support included milder conditions suggested by Glen Research. A 100% ^{15}N enriched phosphoramidite was purchased from Martek and diluted to 1% with unlabeled base. This solution was used to prepare a sample with 1% ^{15}N-labeled at position G4 by synthesis at a 2 μmol scale and purified in the manner described previously. The final concentration of DNA in the samples, calculated from a UV absorbance measurement (at 260 nm), ranged from 1.0 to 1.5 mM per strand. The purity of all samples was assessed by NMR spectroscopy.

NMR Spectroscopy. Experiments were performed on Varian Unity Inova 600 MHz NMR spectrometers. The data sets were processed using Varian software (VNMR), and the real matrixes were transformed to the FELIX (Accelrys, Inc., San Diego, CA) format on Silicon Graphics (Mountain View, CA) Octane workstations. Assignments were based on standard homonuclear NOESY[1] (*9*), DQF−COSY (*10*), TOCSY (*11*), and heteronuclear (^{1}H−^{13}C)HSQC (*12*), (^{1}H−^{15}N)HSQC (*13*), and (^{1}H−^{31}P)HSQC (*14*) experiments. In ^1H_2O, data were acquired with a jump-and-return pulse sequence (*15*) in ^2H_2O at 0, 10, and 20 °C, with Watergate suppression of the residual water signal (*16*) at 20 °C.

Distance and Torsion Restraints. A set of five NOESY mixing times, 50, 100, 150, 200, and 250 ms, was used for build-up curves at 20 °C, with distances estimated from the initial build-up rates of the NOE curves. The interproton distances were estimated using the average of the volume integral of the H1′ to H2″ cross-peaks as 2.20 Å of three chosen residues. Bounds were kept at ±30% and varied widely for overlapping peaks. The cross-peaks were picked manually, and their volumes were integrated using the FELIX (v 2.3) program. Two mixing times (60 and 200 ms) were used to derive distance restraints from the exchangeable protons collected with a jump-and-return NOESY pulse sequence at 0 °C. Distances were considered 3.0 (±0.8) Å for strong peaks, 4.0 (±1.2) Å for medium cross-peaks observed in a 200 ms mixing time spectrum, and 5.0 (±1.8) Å for cross-peaks not observed in a 60 ms mixing time spectrum. Atoms participating in base pairing, as determined based on NOE patterns, were restrained with distances corresponding to ideal hydrogen bond geometry (*17*) (i.e., (G4:G8:G4:G8), (G1:C2:G1:C2:G1), T6:(G3:G7:G3:G7):T6, and A9:A9 shown schematically in Figure 1c−f). Initial stereospecific assignment of individual H2′ and H2″ protons was derived from comparison of intensity of the H1′:H2′ and H1′:H2″ intraresidue cross-peaks in a 50 ms NOESY spectrum and subsequently corroborated by analysis of a DQF−COSY spectrum. A total of 11 dihedral angles per strand were restrained during rMD simulations following analysis of magnetization transfers from sugar pucker protons to backbone ^{31}P as discussed in the Results. The dihedral angle β was restrained to the trans conformation (180 ± 30°) for C2, G4, T5, G7, and A9. The dihedral angle ϵ was restrained to a combination of trans and gauche(−) conformations (−120 ± 55°) for residues G1, G4, T5, T6, G7, and G8. The glycosidic torsion angle χ was restricted to the experimentally observed conformations: syn (45 ± 90°) for residue T5 and anti (220 ± 70°) for all other residues.

Distance Restrained Molecular Dynamics Regularization. Structure calculations were carried out using distance and dihedral angle constraints. Calculations were performed with XPLOR version 3.1 (*18*) and XPLOR−NIH (*19*) using the CHARMm force field (*20*) and adapted for restrained molecular dynamics (rMD) for nucleic acids. All calculations were executed in vacuo without explicit counterions. The initial distance geometry and simulated annealing refinement protocol started from 300 different structures generated from sets of four strands, each 10 nucleotides long, randomized over all dihedral angles. A number of structures (12 out of 300) emerged separated from nonconverged structures by gaps in components of the potential energy function (dihedral angles, van der Waals, NOE violations, and covalent geometry). This set was subsequently submitted to sets of rMD calculations performed using random velocities fitting a Maxwell−Boltzmann distribution following a protocol described previously (*7*). On the basis of the 4-fold sym-

[1] Abbreviations: NOESY, nuclear Overhauser enhancement spectroscopy; TOCSY, total correlation spectroscopy; DQF−COSY, double quantum filtered correlation spectroscopy; HSQC, heteronuclear single quantum coherence; TPPI, time proportional phase increment; WATERGATE, water suppression by gradient tailored excitation; rMD, restrained molecular dynamics.

metry, noncrystallographic symmetry restraints were imposed on all atoms. Weak planarity restraints were also imposed for the pseudo-planar elements (G4:G8:G4:G8), (G1:C2:G1:C2:G1), T6:(G3:G7:G3:G7):T6, and A9:A9 throughout the computations. Coordinates (PDB ID: 1XCE) have been deposited in the PDB data bank.

RESULTS

The d(GCGGTTGGAT) sequence folds into a four-stranded quadruplex with the topology and hydrogen bond alignments shown schematically in Figure 1a,c−f. Proton resonance assignments, folding topology, and high-resolution structure were determined using a combination of through-bond and -space NMR experiments. The process was aided by a number of resonance assignments that were similar to those of the sequence d(GCGGTGGAT) determined at the same pH and salt conditions (*7*). Nevertheless, experimental evidence in support of this multistranded architecture is detailed next.

Nonexchangeable Proton Resonance Assignments. Non-exchangeable ^{1}H, ^{13}C, ^{31}P resonances of d(GCGGTGGAT) were assigned using standard methods (*13*, *21*). Sequential assignments were made on the basis of the H6/H8−H1′ connectivities and proceeded through analysis of the 50 and 250 ms NOESY spectra. These were corroborated by sequential analysis in H6/H8−H3′, by aromatic−aromatic cross-peaks, and in H6/H8−H2′/H2″ connectivities. In Figure 4a, a plot of a NOESY collected with mixing time of 250 ms is shown. The sequential connectivities between the base and its own and 5′-flanking sugar H1′ protons along individual strands can be traced with a couple of interruptions related to one residue. An interruption in the step T5pT6 denoted by lack of the expected intrastrand T6H6−T5H1′ cross-peak, with an associated very strong T6H6−T6H1′ indicates that the glycosidic torsion angle χ for T6 is syn, or close to it. In fact, the C1′−H1′ bond may be expected to be close to perpendicular to the base-plane because the cross-peak G7H8−T6H1′ is also faint, and the sequential cross-peaks T5H6−T6H6, T5H6−T6H5, and T5H5−T6H6 are not observed even at 250 ms. This is indicative of a distance over 5.1 Å between T6H1′ and either G7H8 and T5H6.

The initial assignment of A8H2 was initially derived from the typical intraresidue A9H1′−A9H2 and observation of T9H1′−A8H2 connectivities (Figure 4a). Corroboration of assignments of ^{1}H resonances followed analysis of the characteristic chemical shifts of attached ^{13}C. Further evidence for assignment of sugar H3′ and some H4′/H5′/H5″ was achieved through analysis of their magnetization transfers to backbone ^{31}P, which are also sequential in nature: H3′(i-1)-P(i-1)-H4′/H5′/H5″(i) (Figure 4b). Dihedral angle constraints were derived from some of the heteronuclear couplings (*13*, *22*). Absence of $^{3}J_{H5'/5''-P}$ in this spectrum represents a coupling constant magnitude smaller than 5 Hz; thus, β was loosely constrained to the trans conformation ($180 \pm 30°$) for C2, G4, T5, G7, and A9. Furthermore, since $^{3}J_{H3'-P}$ is clearly observable (>5 Hz coupling constant) for residues G1, G4, T5, T6, G7, and G8 ϵ and can be both trans and gauche(−), these residues were restrained to $-120 \pm 55°$. Because cross-peaks for residues C2 and A9 were somewhat weaker, they were not constrained.

Hydrogen Bond Alignments and Topology. By modifying the sequence d(GCGGTGGAT) with addition of thymine T6,

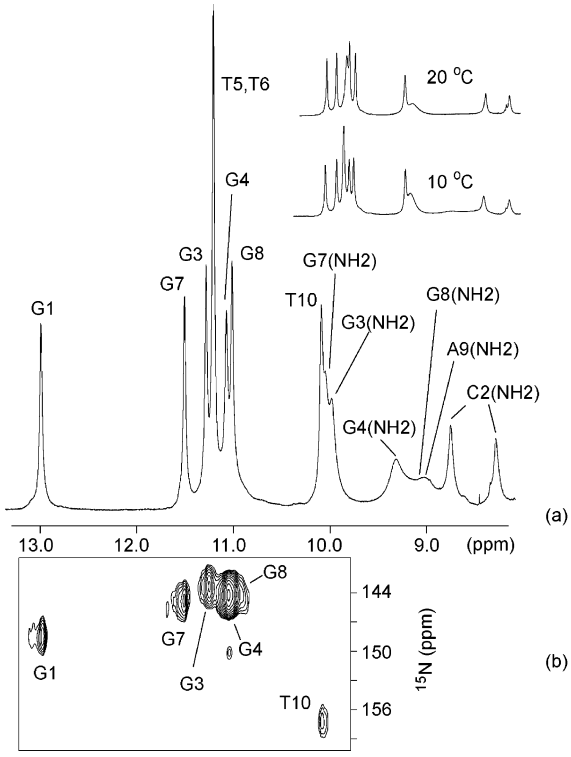

FIGURE 2: (a) Proton NMR spectrum (8.0−13.5 ppm) of d(GCGGTTGGAT) in 100 mM NaCl, 5 mM phosphate, $^{1}H_2O$, at pH 6.8 and 0 °C. Expansions of the exchangeable region at 10 and 20 °C are also shown on top. The assignments of the imino and amino protons are listed over the resonances at 0 °C. (b) An [^{1}H,^{15}N] HSQC spectrum recorded in $^{1}H_2O$ at 10 °C. Five high field imino-bound ^{15}N chemical shifts appear in a region characteristic of guanine imino, and only one signal appears in the region characteristic for thymine imino. The stronger peak for G4 is due to the fact that ^{15}N for this residue was enriched by 1%.

it was expected that the topological architecture would be maintained. Indeed, peaks 1 (G7H8−G1H1′), 2 (G7H8−G1H8), 4 (C2H6−G1H8), and 5 (G1H8−G7H1′) in Figure 4a are a signature feature for the expected topological architecture (*7*) indicating the nature of the dimeric interface. In Figure 2, the imino proton spectrum of d(GCGGTTGGAT) sequence in 100 mM NaCl, pH 6.8 at 0 °C is shown. In the 8.4−12.9 ppm exchangeable proton region, 12 resonances are identifiable (including isochronous signals at ∼11.2 ppm). The number of sharp resonances in the 10.0−12.9 ppm imino proton region coincides with the sum of guanines and thymines in the sequence, thus suggesting the formation of a structure with symmetry related strands. The isochronous signals split at higher temperatures, as observed from Figure 2a, for which some of the proton dipolar interactions for these signals are no longer observable at both 200 or 60 ms mixing times. Their appearance at ∼11.2 ppm indicates possible participation in hydrogen bond formation since unpaired TH3 protons typically appear at approximately 10 ppm. The identification of guanine imino protons is corroborated by the detection of their one-bond correlations with attached imino ^{15}N, which fall in a characteristic region, 143−149 ppm (Figure 2b). The guanine imino G4H1 was distinguished from other resonances from its intensity due to the fact that the sample was 1% ^{15}N-labeled site specifically. The resonance at ∼157 ppm falls in a region characteristic for thymine ^{15}N imino resonances and is correlated to a proton at 10.3 ppm. A thymine imino proton

peak in that region indicates that possibly it is not forming hydrogen bonds in a canonical A:T base-pair. The fact that both T6H3 and T5H3 do not appear in this spectrum implies that the one bond coupling $^1J_{H-N}$ is significantly different from 90 Hz (2.78 ms was used for the one bond coherence transfer), or that their chemical shifts are significantly downfield shifted since the ^{15}N carrier was set to ~150 ppm, or both. Both are also suggestive of hydrogen bond formation for these residues. The appearance of resonances in the 10.7−11.6 ppm region is characteristic of N−H:N hydrogen bond alignment associated with G:G:G:G tetrad formation (*2*, *23*). The remaining guanine proton resonates in a region characteristic of N−H:O═C hydrogen bond alignment characteristic of Watson−Crick G:C pair formation associated with G:C:G:C tetrad formation. Assignment of amino protons observed in Figure 2a followed from their strong NOE connectivities to imino and aromatic protons.

Figure 1c−f depicts the hydrogen-bonding alignments that make up the global architecture. Patterns of NOEs characteristic for the formation of each of the pseudo-planar elements were observed in the JR−NOESY (60 and 200 ms mixing times) data sets. The G1:C2:G1:C2 tetrad is characterized by cross-peak G1H1−C2H41/H42 (5 in Figure 3) and the associated observation of a strong G1H8−C2H5 cross-peak, thus indicating G:C pairing through the Hoogsteen edge of guanine. These observations verify the direct alignment of opposing Watson−Crick G1:C2 pairs through their major groove edges. The directionality of the G3:G7:G3:G7 tetrad formation is given by the observation of cross-peaks of amino and imino of G3 to H8 of G8 (peaks 8 and 41 in Figure 3), and correspondingly, amino and imino of G8 to H8 of G3 (peaks 13 and 43). The observation of cross-peaks between the imino of T6 and G3H22 and G3H21 (peaks 16 and 21, respectively) are indicative of the possibility for hydrogen bond formation through the minor groove edge of G3 as shown schematically in Figure 1d. The relative positioning and alignment of T6 are further corroborated by cross-peaks T6H3−G7H8 (peak 20) and T6H3−G1H1′ (peak 17), which show that the Watson−Crick edge of T6 points toward the quadruplex stem. Superposition of G1:C2:G1:C2 tetrad and T6:(G3:G7:G3:G7):T6 hexad is further indicated by a number of cross-peaks in the JR−NOESY at 200 ms in Figure 3 (peaks 7, 9, 12, 14, 40) and NOESY at 250 ms in Figure 4a (peaks 1, 2, 4, 5).

In Figure 3, both imino and amino protons of G4 show cross-peaks to H8 of G8 (peaks 25 and 46, respectively), and the imino proton of G8 shows cross-peaks to H8 of G4 (peak 31). These along with other cross-peaks were sufficient to characterize G4:G8:G4:G8 tetrad formation since cross-peaks for the amino of G8 is not observed due to a fast exchange regime for G8NH2 for both 200 (Figure 2) and 60 ms mixing times. At the lower mixing time, a cross-peak connecting the amino of G8 is observed (not shown). Because of a more solvent exposed tetrad, much broader signals are observed for both the amino of G4 and the amino of G8, as seen in Figure 2. The stacking of G4:G8:G4:G8 and T6:(G3:G7:G3:G7):T6 is indicated by some cross-peaks appearing in Figure 3 (peaks 24, 27, 33, 35, 45). It is noteworthy that for both uracil substituted sequences, the T:(G:G:G:G):T hexad hydrogen bond alignment does not succeed even though there are indications that the topological architecture is maintained. The assignments of cross-peaks

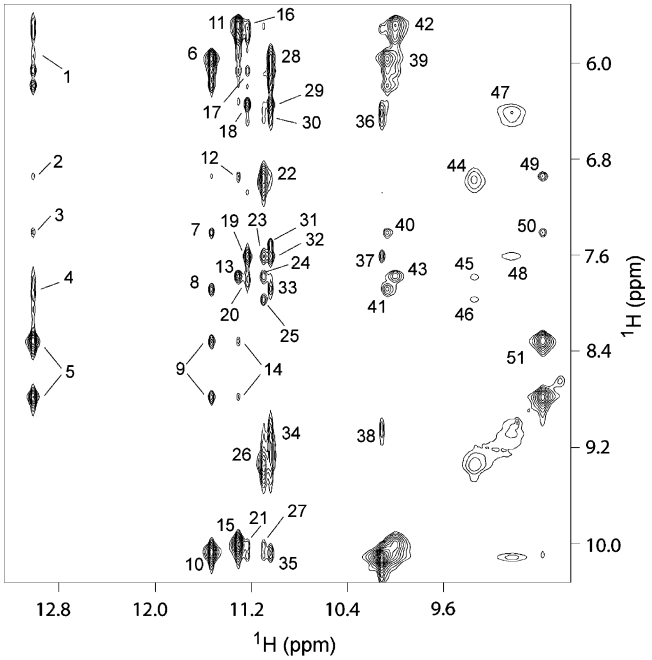

FIGURE 3: Expanded JR−NOESY spectrum (200 ms) of d(GCGGTTGGAT) in 100 mM NaCl, 5 mM sodium phosphate buffer at pH 6.8 in ^1H_2O at 0 °C, exhibiting dipolar connectivities between imino and aromatic protons. Peaks 1−50 are assigned as follows: (1) G1H1−G1H22, (2) G1H1−G1H8, (3) G1H1−C2H6, (4) G1H1−G1H21, (5) G1H1−C2H41/42, (6) G7H1−G7H22, (7) G7H1−C2H6, (8) G7H1−G3H8, (9) G7H1−C2H41/42, (10) G7H1−G7H21, (11) G3H1−G3H22, (12) G3H1−G1H8, (13) G3H1−G7H8, (14) G3H1−C2H41/42, (15) G3H1−G3H21, (16) T6H3−G3H22, (17) T6H3−G1H1′, (18) T5H3−A9H1′, (19) T5H3−A9H2, (20) T6H3−G7H8, (21) T6H3−G3H21, (22) G4H1−G4H22, (23) G4H1−A9H2, (24) G4H1−G7H8, (25) G4H1−G8H8, (26) G4H1−G4H21, (27) G4H1−G3H21, (28) G8H1−G8H22, (29) G8H1−A9H1′, (30) G8H1−A9H62, (31) G8H1−G4H8, (32) G8H1−A9H2, (33) G8H1−G3H8, (34) G8H1−G8H21, (35) G8H1−G7H21, (36) T10H3−A9H62, (37) T10H3−A9H2, (38) T10H3−A9H61, (39) G7H21−G7H22, (40) G7H21−C2H6, (41) G7H21−G3H8, (42) G3H21−G3H22, (43) G3H21−G7H8, (44) G4H21−G4H22, (45) G4H21−G7H8, (46) G4H21−G8H8, (47) A9H61−A9H62, (48) A9H61−A9H2, (49) C2H41−G1H8, (50) C2NH41−C2H6, and (51) C2H41−C2H42.

for the isochronous imino of T5 and T6 were done from cross-peaks observed in JR−NOESY (200 ms) at 10 °C. They were further aided by analysis of the same experiment under the same conditions for samples in which T5 and T6 were substituted for uracil- d(GCGGUTGGAT) and d(GCGGTUGGAT), respectively. In both cases, the topological architecture is maintained, but not all hydrogen bond alignments are maintained. The substitution of T6 for uracil forms the same topological fold with the distinction that the U6 imino resonance is not observable. Instead, T5 forms contacts to A9 (T5H3−A9H2, T5H3−A9H1′, Supporting Information, NOESY 200 ms) as observed for T5 in the unsubstituted sequence. By T5 being substituted for uracil, both exchangeable protons (T6H3 and U5H3) are not observable in 200 ms 11-NOESY at 0 °C.

Assignment of the A9:A9 mismatch is principally supported by the observation of cross-peaks of the amino to A9H2 (peak 48 is shown in Figure 3). This is only possible if the cross-peak is an interresidue, thus reflecting a Watson−Crick edge mismatch; see, for example, Figure 1d. The difference in chemical shifts between the amino protons also suggests that only one of the amino is bound—$\Delta\delta$ 2.3 ppm

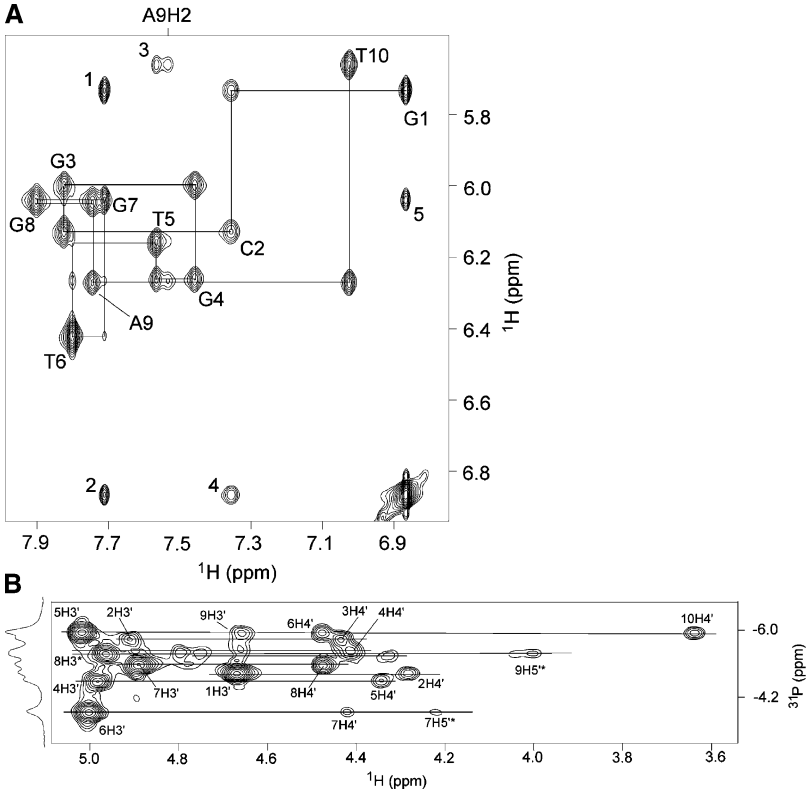

FIGURE 4: (a) Expanded NOESY (250 ms mixing time) spectrum recorded in ^2H_2O at 20 °C correlating the aromatic base proton and sugar H1′ for d[(GCGGTTGGAT)$_2$]$_2$. The line traces the NOE connectivities between the base protons and their own and 5′-flanking sugar H1′ protons from G1 to T10 in the sequence. The interruptions in the steps T5pT6 and T6pG7 denoted by weak cross-peaks T5H1′−T6H6 and T6H1′−G7H8, respectively, with the concomitant very strong cross-peak T6H6−T6H1′, indicate a syn glycosidic bond angle with the C1′−H1′ bond close to perpendicular to the base-plane. Cross-peaks G7H8−G1H1′ (peak 1), G1H8−G7H8 (peak 2), G1H8−G7H1′ (peak 5), and C2H6−G1H8 (peak 4) are crucial assignments leading to the identification of the architecture of the quadruplex formed by the sequence d(GCGGTTGGAT) in Na^+ salt solution. Cross-peak T5H6−T10H1′ (peak 3) indicates the relative positioning of the looping residue T5. (b) A [^{31}P−^{1}H] correlation spectrum of d(GCGGTTGGAT) in 100 mM NaCl (pH 6.8) at 20 °C showing assignments that allowed for the derivation of angular constraints.

(cross-peak 47), which is precisely the same magnitude as for the A:A mismatch in the d(GCGGTGGAT) sequence. However, in contrast to the structure formed by the sequence d(GCGGTGGAT), here we observe juxtaposition of T10 and A9. This is illustrated by cross-peaks T10H3−A9H62 (peak 36), T10H3−A9H2 (peak 37), and T10H3−A9H61 (peak 38). These cross-peaks are also illustrative of the relative disposition and orientation of the Watson−Crick edge for both T10 residues and reflect a possible T10/T10 platform. The stacking of T10 and A9 is corroborated by the lack of cross-peaks between T10 and any of the residues of the G4:G8:G4:G8 tetrad in the range of mixing times measured in NOESY experiments in ^1H_2O. Because the chemical shift of T10H3 appears in a chemical shift region that is characteristic for free (nonbase paired) thymines, no empirical hydrogen bonding restraints or planarities were imposed during structure calculations. The disposition of thymine T10 appears to be influenced by the looping residue T5, as suggested by numerous cross-peaks (for example, T5H6−T10H1′, peak 3 in Figure 4a). The relative disposition of thymine T5 is further illustrated by cross-peaks T5H3−A9H1′ (peak 18 in Figure 3) and T5H3−A9H2 (peak 19 in Figure 3). This positions the Watson−Crick edge of T5 pointing toward the major groove side of the backbone region of the step G8pA9 and suggests the possibility of hydrogen bond stabilization through hydrogen bond acceptors of the sugar puckers or backbone.

Table 1: NMR Restraints and Structural Statistics for Seven Selected Structures for the Dimeric d(GCGGTTGGAT) Quadruplex

NMR Restraints	
total number of restraints	339
nonexchangeable protons	202
exchangeable protons	68
hydrogen bond restraints (empirical)	48
phosphodiester torsion angle restraints[a]	11
glycosidic torsion angle restraints[a]	10
noncrystallographic symmetry restraints on all heavy atoms	
Structural Statistics	
NOE rmsd (Å) total	0.022 ± 0.008
NOE violations exceeding 0.2 Å	0
deviations from ideal covalent geometry, rmsd	
bond lengths (Å)	0.016 ± 0.001
gond angles (deg)	4.45 ± 0.03
impropers (deg)	0.49 ± 0.04
pairwise all heavy atoms rmsd (Å)	0.9 ± 0.2

[a] Number of restraints per strand.

Structural Features. The applied constraints and structural statistics for the seven final structures are summarized in Table 1. The root-mean-square deviations (rmsd) versus the mean structure for all heavy atoms were 0.9 ± 0.2 Å. Figure 5a shows a stereoview of the superposition of the seven final structures. A representative structure with the lowest energy is depicted with a trace of the backbone main chain in Figure 5b. Shallow turns for the double chain reversal are apparent. In Figure 5c, a view from the top for

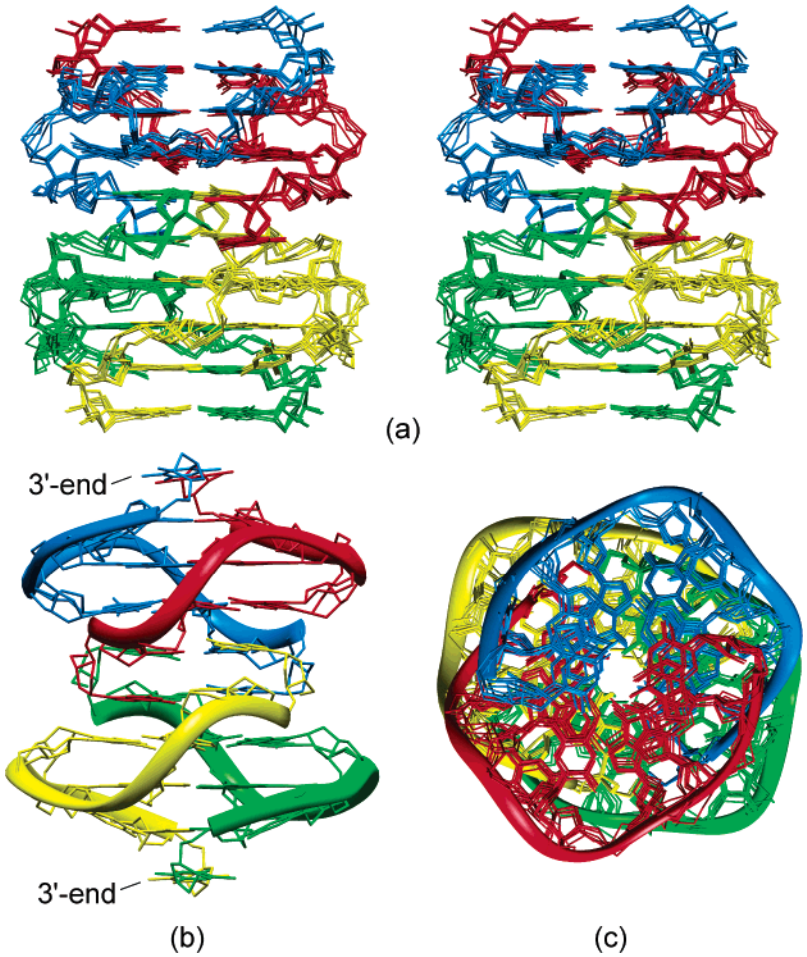

FIGURE 5: (a) Stereoview of a superposition of seven refined structures of the quadruplex formed by the sequence d(GCGGTTGGAT) in sodium solution. The individual strands are yellow, cyan, green, and red. Protons and the exocyclic phosphate oxygens were deleted for clarity. (b) A stick depiction of the backbone of the lowest energy refined structure of the quadruplex motif. (c) A top view of the aligned seven lowest energy refined structures.

the seven final structures is depicted with a trace of the backbone main chain for the lowest energy structure. From the top view, the hexad motif modulates widening of the otherwise circular quadruplex toroid toward a rectangular shape. This shape is due to the hexad alignment. The alignment of two G3(T6−G7) triads into a hexad pseudo-planar element is shown in Figure 6a,b. The recognition of the sheared edge of G3 by the Watson−Crick edge of T6 is apparent. This feature results from the single-stranded double chain reversal within the segment GGTTGG (G3−G8) as depicted in Figure 6b. Notably, the chemical shifts for T5 and G6 in the double chain reversal deviate by more than 1 ppm from normal backbone angles (e.g., in comparison to the terminal G1). Accordingly, for both residues, the dihedral angle ζ is trans even though it was not restrained during simulations. In Figure 6a, the stacking of T5:(G3:G7:G3:G7):T5, G4:G8:G4:G8, and T5 is depicted. It shows that the hexad base T6 is stacked to the deoxyribose moiety of T5. Indeed, the O4′ of the sugar pucker points to the center of the pyrimidine denoting the possibility for a η-type interaction between O4′ and electron delocalization of the pyrimidine.

Figure 6b depicts the disposition and alignment of T5O4 to the amino proton of A9. The feature is well-established from the numerous T5−T10 and some T5−A9 NOE connectivities. It is noteworthy that no planarities or hydrogen bonds were used to restrain the T10/T10 platform shown in Figure 6c. In this figure, both the T5:A9:A9:T5 hydrogen bond alignment and the juxtaposed T10/T10 platform are evident and show good base-stacking interactions. This tetrad alignment shown schematically in Figure 1f was not anticipated from proton connectivities between intervening bases since both amino protons of A9 were too broad. However, the T5H3−A9H1′ and T5H3−A9H2 cross-peaks (respectively, peaks 18 and 19 in Figure 3) are observable. The downfield shift of T5H3 could thus be due to the fact that, by having T5 as part of a pseudo-planar element, this proton falls in a deshielding region of the aromatic isotropic magnetic field of its base-paired A9 (Figure 6a). However, a water molecule could also mediate hydrogen bonding to the A9 backbone. Good base stacking is observed for the Watson−Crick edge A9:A9 mispair alignment of the T5:A9:A9:T5 tetrad and T10/T10. The T5 bases show departure from coplanarity with the mismatch. The hydrogen bond directionalities in all pseudo-planar elements are anticlockwise, except for the juxtaposed G1:C2:G1:C2 tetrads at the dimeric interface. The T10/T10 platform is aligned in a disposition appropriate for a T:T wobble pair. But, in any of the selected seven structures, the atoms are within hydrogen bonding distance (consistent with their T10H3 imino chemical shift).

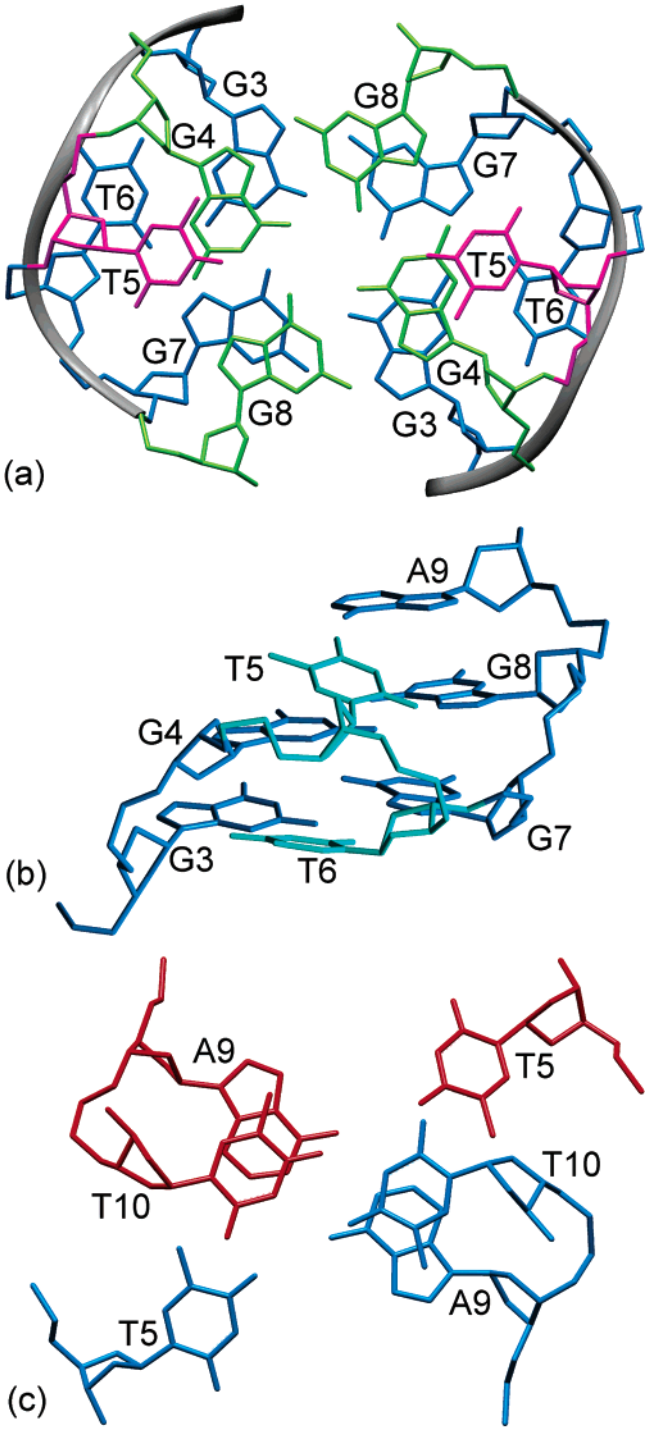

FIGURE 6: Depictions of structural details for a representative refined structure of d[(GCGGTTGGAT)$_2$]$_2$. (a) Stacking depictions between T5:(G3:G7:G3:G7):T5 in blue, G4:G8:G4:G8 in green, and thymine T5 in pink. (b) View of the double chain reversal depicting disposition of its interspersed thymines in lighter blue: thymine T5 vis-a′-vis A9 and the triad G3(T6-G7). (c) Juxtaposition of T5:A9:A9:T5 tetrad and T10/T10 platform. The two symmetrical strands are depicted in red and blue.

DISCUSSION

Principles for the formation of higher order architectures are to be established through the observation of recurring structural motifs associated with particular DNA sequences. Identification of new pairing alignments generally involves the screening of numerous DNA sequences. By building into an established framework topology, we have here explored the possibility for design of new architectural features. Thus, in an effort to move from serendipity to design, we are systematically investigating the robustness of double chain reversals bridging tetrad layers using as a starting point the topology formed by the sequence d(GCGGTGGAT) in sodium at pH 6.8 (*7*) (Figure 1b). In the structure formed by this sequence, the segment GGTGG undergoes a double chain reversal in which the interspersed thymine in the syn conformation loops out, resulting in its methyl group being buried into the quadruplex stem and a solvent exposed Watson−Crick edge. By varying the nature of residues bracketed by a couple of GpG steps by inserting more than one residue between the two GpG steps, it is possible to probe the versatility of the double chain reversals and demonstrate experimentally novel pairing alignments.

Here, we have established that the topology is sufficiently robust and the preferred folding topology for the sequence d(GCGGTTGGAT). It has served for the experimental demonstration for formation of both a G(T−G) triad and an A:A Hogsteen edge mispair aligned T:A:A:T tetrad in a quadruplex.

The double chain reversal in the GGTTGG segment forms a hitherto unidentified base triad G3(T6−G7) in which the sheared edge of a guanine is recognized by the Watson−Crick edge of a looping thymine as shown schematically in Figure 6b. Since both guanines of the triad are part of a G-tetrad in a symmetrical bi-stranded dimer as shown in Figure 5, their platform results in the unprecedented T6:(G3:G7:G3:G7):T6 hexad alignment shown schematically in Figure 1d. This alignment was the feature anticipated with the insertion of a thymine into the GGTGG segment. Thus far, pseudo-planar structured elements with more than four bases are known only for adenines recognizing the sheared edge of guanines part of G-tetrads, thus forming pentads, hexads, and heptads (*4*−*6*, *24*). These pseudo-planar architectures stem from the assembly of the G(A−G) triad as a recurring motif in GGAGG segments.

An unanticipated feature was the formation of a pseudo-planar architecture involving the remaining looping thymine. In the original structure with this topology, a Watson−Crick edge A:A mismatch served a capping function to the quadruplex stem by forming a platform across the quadruplex toroid (*7*). This disposition is also found in the present structure. Consequently, the wide open Hoogsteen edges were ideal for recognition by the looping T5. In the current structure, T5O4 forms a hydrogen bond to the remaining amino proton donor of A9, resulting in the T5:A9:A9:T5 tetrad shown schematically in Figure 1f. The formation of other tetrad pairing alignments involving pairs of adenines and thymines has been previously demonstrated (*25*, *26*). The known T:A:T:A tetrad alignment in a quadruplex results from Hoogsteen edge mispair alignment of adenines forming part of a pair of Watson Crick A:T base pairs (*26*). This has as a consequence a slipped alignment at the end of a quadruplex stem. In contrast, the formation of T10/T10 platform stacking on the A9:A9 mismatch in the current structure indicates that progression of the strands as a regular double helix is favorable. Thus, this four-stranded topology suggests a pathway for recombination events involving the association of quadruplex entities with GpC dangling ends (*7*, *27*).

Comparisons of Double Chain Reversal Loops. In spanning G-tetrads, the conformation diversity of double chain reversal loops is sensitive to the nature of nucleotide, nucleotide sequence, and solution conditions among other factors. By comparing DNA quadruplex structures bearing double-chain reversals, it is possible to infer constraints leading to their formation and stabilization. Thus, we are currently examining both stability and impact of the nature and number of the looping residues within the same topological framework utilizing solution NMR methods. Notably, caution is required for correctly restraining backbone dihedral angles from NMR structural studies. Accordingly, for the current study, we have made conservative choices for the use of dihedral angle restraints derived from ^{31}P to ^{1}H correlations and did not use coupling constraints to further restrain sugar puckers.

In general, canonical B and A-DNA dihedral angles populate preferentially gauche (−) for α and ζ, gauche (+) for γ, and trans for β and ϵ (*17*) conformations. Deviations from canonical conformations were found for the double chain reversal in the GGAGG segment in which the interspersed adenine populates preferentially α(g+), β(t∼g−) and γ(t) (*6*). The syn thymine in GGTGG loops out (*7*) and populates different conformations: α(g−), β(g+), and γ(+). In the segment GGTTGG, both thymines also populate α(g−)γ(g+), the syn T6 is also β(g+), but the anti T5 populates preferentially β(t) (Table S1 in Supporting Information). An illustration of the results of the concomitant backbone mechanics for these three cases is presented in Figure 7a−c. The most salient feature for double chain reversals with interspersed thymines is that instead of the typical ϵ(t)ζ(g−) torsion domains being populated; both in GGTTGG and in GGTGG (*7*) their preferred conformations are ϵ(g−)ζ(t).

Both interspersed thymines in the double chain reversal spanning three G-tetrad layers in the GGTTGG segment of the solution structure formed by four TTGGGG loop out (*28*) (Figure 7f). This is analogous to the segment GGTGG (*7*), in which a double chain reversal spans two G-tetrad layers as shown in Figure 7a. But, interestingly, in a double chain reversal spanning two G-tetrad layers observed in the segment GGCAGG (*29*), both interspersed residues (the cytosine and the adenine) do not form pseudo-planar architectures (Figure 7d). The same is true for the interspersed ATT in the structure of the human telomeric sequence by Parkinson et al. (*30*) bearing a GGATTGG segment (Figure 7e). In this case, the double chain reversal spans three tetrad layers as in the segment GGGTTGGG of the tetrahymena telomeric sequence (*28*). In all three cases, the looping bases are accessible to form hydrogen bonds and recognition by other biomolecules. Contrasting with the tetrahymena telomeric sequence, in the current structure all residues in the GGTTGG segment are involved in the formation of pseudo-planar elements. The first thymine in the segment does in fact form a further tetrad layer consistent with a virtually normal progression of the backbone. Thus, the single T5−A9 hydrogen bond is possible with a small deviation from the tetrad plane by T5 as depicted in Figure 6b. Accordingly, the next step effectively spans three tetrad layers. It is the backbone in the steps T5pT6 and T6pG7 that appear to mostly accommodate the deformations. In comparison, in the loop in the human telomeric sequence

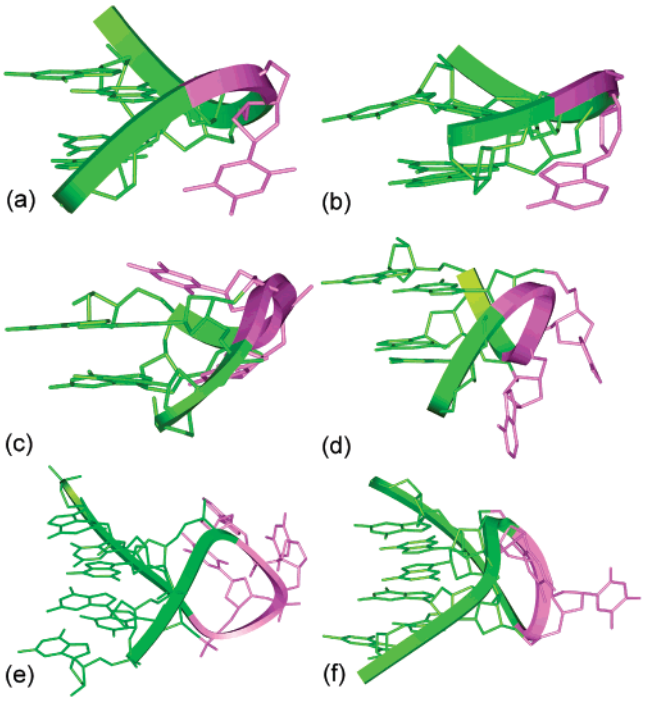

FIGURE 7: Depictions of double chain reversals (a) the GGTGG segment of the sequence d(GCGGTGGAT) (PDB ID: 1NYD (*7*)), (b) a GGAGG segment of the sequence d(GGA)$_8$ (PDB ID: 1OZ8 (*24*)), (c) the GGTTGG segment of the sequence d(GCGGTTGGAT) (PDB ID: 1XCE), (d) the GGCAGG segment of the sequence d(G$_2$T$_4$GGCAGGGT$_4$G$_2$T) (PDB ID: 1I34 (*29*)), (e) the GGTTAGG segment of the sequence d[(AGGGTTA)$_3$AGGG] (PDB ID: 1KF1 (*30*)), and (f) a GGTTGG segment of the d(TTGGGG)$_4$ sequence (PDB ID: 186D (*28*)). The interspersed looping residues are in pink.

by Parkinson et al. (*30*), the deformations for the double chain reversal are spread throughtout five residues (GTTAG) that seem to be sufficient to accommodate a full local backbone helicoidal turn as shown in Figure 7e. An even more strained loop has been observed in the folding topology for the sequence d(G$_3$T$_4$G$_4$) in solution (*31*). In this case, just the backbone spans three layers of G-tetrads (i.e., the tetrad pseudo-planar elements of each of guanines in the GpG step are juxtaposed to an interceded G-tetrad). However, this loop is not part of a double chain reversal resulting in contiguous parallel strands.

Biological Implications. There is a well-established interest in identifying topologies associated with sets of G-tracks interrupted by adenines, thymines, or both mediating double chain reversals since they seem prevalent in biologically significant regions (*8*, *30*, *32*−*39*). Because the structural plasticity of DNA is inextricably connected to its biological function, we need more detailed information about the structural impact of nucleotide sequence variation. Since loops are a determinant feature of higher order architecture, identification of the diversity of conformation they cover greatly enlarges the repertoire of principles for formation and stability of interesting topologies. Turns, loops, and pseudo-planar motifs in higher order architectures can be recognizable structural motifs lending uniqueness to possible accessible topologies, in particular, genomic regions. This type of structural knowledge allows for selectivity and specificity in targeting modulation of topologies for therapeutic purposes (*32*, *35*, *40*). Comprehensive coverage of

all stable, and transient, structural elements may allow for the prediction of topologies associated with sequences of biological significance.

ACKNOWLEDGMENT

I am indebted to Prof. Laurence H. Hurley and his group for stimulating discussions and to anonymous referees for their constructive criticism.

SUPPORTING INFORMATION AVAILABLE

Table with backbone torsion angles for the lowest energy calculated structure as well as one figure showing a JR−NOESY (200 ms) at °C for 5′-GCGGUTGGAT-3′ at pH 6.8. This material is available free of charge via the Internet at http://pubs.acs.org.

REFERENCES

1. Kang, C., Zhang, X. H., Ratliff, R., Moyzis, R., and Rich, A. (1992) Crystal Structure of 4-Stranded Oxytricha Telomeric DNA, *Nature 356*, 126−131.
2. Smith, F. W., and Feigon, J. (1992) Quadruplex structure of Oxytricha telomeric DNA oligonucleotides, *Nature 356*, 164−8.
3. Wang, Y., and Patel, D. J. (1995) Solution structure of the Oxytricha telomeric repeat d[G4(T4G4)3] G-tetraplex, *J. Mol. Biol. 251*, 76−94.
4. Zhang, N., Gorin, A., Majumdar, A., Kettani, A., Chernichenko, N., Skripkin, E., and Patel, D. J. (2001) V-shaped scaffold: a new architectural motif identified in an A × (G × G × G × G) pentad-containing dimeric DNA quadruplex involving stacked G(anti) × G(anti) × G(anti) × G(syn) tetrads, *J. Mol. Biol. 311*, 1063−79.
5. Kettani, A., Gorin, A., Majumdar, A., Hermann, T., Skripkin, E., Zhao, H., Jones, R., and Patel, D. J. (2000) A dimeric DNA interface stabilized by stacked A:(G:G:G:G):A hexads and coordinated monovalent cations, *J. Mol. Biol. 297*, 627−44.
6. Matsugami, A., Ouhashi, K., Kanagawa, M., Liu, H., Kanagawa, S., Uesugi, S., and Katahira, M. (2001) An intramolecular quadruplex of (GGA)(4) triplet repeat DNA with a G:G:G:G tetrad and a G(:A):G(:A):G(:A):G heptad and its dimeric interaction, *J. Mol. Biol. 313*, 255−69.
7. Webba da Silva, M. (2003) Association of DNA Quadruplexes through G:C:G:C:G Tetrads. Solution Structure of d(GCGGTGGAT), *Biochemistry 42*, 14356−14365.
8. Grand, C. L., Powell, T. J., Nagle, R. B., Bearss, D. J., and Hurley, L. H. (2003) Identification of a G to A mutation in the c-MYC repressor element that results in inactivation of the G-quadruplex repressor element and overexpression of c-MYC in human colorectal cancer, *Clin. Cancer Res. 9*, 6125S.
9. Jeener, J., Meier, B. H., Bachmann, P., and Ernst, R. R. (1979) Investigation of Exchange Processes by 2-D NMR Spectroscopy, *J. Chem. Phys. 71*, 4546−4553.
10. Piantini, U., Sorensen, O. W., and Ernst, R. R. (1982) Multiple Quantum Filters for Elucidating NMR Coupling Networks, *J. Am. Chem. Soc. 104*, 6800−6801.
11. Braunschweiler, L., and Ernst, R. R. (1983) Coherence Transfer by Isotropic Mixing−Application to Proton Correlation Spectroscopy, *J. Magn. Reson. 53*, 521−528.
12. Bodenhausen, G., and Ruben, D. J. (1980) *Chem. Phys. Lett. 69*, 185−188.
13. Varani, G., Abouela, F., and Allain, F. H. T. (1996) NMR investigation of RNA structure, *Prog. Nucl. Magn. Reson. Spectrosc. 29*, 51−127.
14. Sklenar, V., Miyashiro, H., Zon, G., Miles, H. T., and Bax, A. (1986) Assignment of the ^{31}P and ^{1}H resonances in oligonucleotides by two-dimensional NMR spectroscopy, *FEBS Lett. 208*, 94−98.
15. Gueron, M., and Plateau, P. (1982) Exchangeable proton NMR without baseline distortion, using new strong-pulse sequences, *J. Am. Chem. Soc. 104*, 7310−7311.
16. Piotto, M., Saudek, V., and Sklenar, V. (1992) Gradient-Tailored Excitation for Single-Quantum NMR Spectroscopy of Aqueous Solutions, *J. Biomol. NMR 2*, 661−665.
17. Saenger, W. (1984) *Principles of Nucleic Acid Structure*, Springer-Verlag, Inc., New York.
18. Brunger, A. T. (1992) Ph.D. Thesis, Department of Molecular Biophysics and Biochemistry, Yale University, New Haven.
19. Schwieters, C. D., Kuszewski, J. J., Tjandra, N., and Clore, G. M. (2003) The Xplor-NIH NMR Molecular Structure Determination Package, *J. Magn. Reson. 160*, 66−74.
20. Brooks, B. R., Bruccoleri, R. E., Olafson, B. D., States, D. J., Swaminathan, S., and Karplus, M. (1983) CHARMM: A program for macromolecular energy minimization and dynamics calculations, *J. Comput. Chem. 4*, 187−217.
21. Wüthrich, K. (1986) *NMR of Proteins and Nucleic Acids*, John Wiley & Sons Inc., New York.
22. Wijmenga, S. S., and van Buuren, B. N. M. (1998) The use of NMR methods for conformational studies of nucleic acids, *Prog. Nucl. Magn. Reson. Spectrosc. 32*, 287−387.
23. Wang, Y., and Patel, D. J. (1993) Solution Structure of the Human Telomeric Repeat D Ag(3)(T(2)Ag(3))3 G-Tetraplex, *Structure 1*, 263−282.
24. Matsugami, A., Okuizumi, T., Uesugi, S., and Katahira, M. (2003) Intramolecular higher order packing of parallel quadruplexes comprising a G:G:G:G tetrad and a G(:A):G(:A):G(:A):G heptad of GGA triplet repeat DNA, *J. Biol. Chem. 278*, 28147−28153.
25. Salisbury, S. A., Wilson, S. E., Powell, H. R., Kennard, O., Lubini, P., Sheldrick, G. M., Escaja, N., Alazzouzi, E., Grandas, A., and Pedroso, E. (1997) The bi-loop, a new general four-stranded DNA motif, *Proc. Natl. Acad. Sci. U.S.A. 94*, 5515−8.
26. Zhang, N., Gorin, A., Majumdar, A., Kettani, A., Chernichenko, N., Skripkin, E., and Patel, D. J. (2001) Dimeric DNA quadruplex containing major groove-aligned A−T−A−T and G−C−G−C tetrads stabilized by intersubunit Watson−Crick A−T and G−C pairs, *J. Mol. Biol. 312*, 1073−88.
27. Sen, D., and Gilbert, W. (1990) A Sodium−Potassium Switch in the Formation of 4-Stranded G4-DNA, *Nature 344*, 410−414.
28. Wang, Y., and Patel, D. J. (1994) Solution structure of the Tetrahymena telomeric repeat d(T2G4)4 G-tetraplex, *Structure 2*, 1141−56.
29. Kuryavyi, V., Majumdar, A., Shallop, A., Chernichenko, N., Skripkin, E., Jones, R., and Patel, D. J. (2001) A double chain reversal loop and two diagonal loops define the architecture of a unimolecular DNA quadruplex containing a pair of stacked G(syn)−G(syn)−G(anti)−G(anti) tetrads flanked by a G− (T−T) Triad and a T−T−T triple, *J. Mol. Biol. 310*, 181−94.
30. Parkinson, G. N., Lee, M. P., and Neidle, S. (2002) Crystal structure of parallel quadruplexes from human telomeric DNA, *Nature 417*, 876−80.
31. Cmugelj, M., Sket, P., and Plavec, J. (2003) Small change in a G-rich sequence, a dramatic change in topology: New dimeric G-quadruplex folding motif with unique loop orientations, *J. Am. Chem. Soc. 125*, 7866−71.
32. Hurley, L. H. (2002) DNA and its associated processes as targets for cancer therapy, *Nat. Rev. Cancer 2*, 188−200.
33. Hurley, L. H. (2001) Secondary DNA structures as molecular targets for cancer therapeutics, *Biochem. Soc. Trans. 29*, 692−6.
34. Grand, C. L., Powell, T. J., Nagle, R. B., Bearss, D. J., Tye, D., Gleason-Guzman, M., and Hurley, L. H. (2004) Mutations in the G-quadruplex silencer element and their relationship to c-MYC overexpression, NM23 repression, and therapeutic rescue, *Proc. Natl. Acad. Sci. U.S.A. 101*, 6140−5.
35. Siddiqui-Jain, A., Grand, C. L., Bearss, D. J., and Hurley, L. H. (2002) Direct evidence for a G-quadruplex in a promoter region and its targeting with a small molecule to repress c-MYC transcription, *Proc. Natl. Acad. Sci. U.S.A. 99*, 11593−8.
36. Seenisamy, J., Siddiqui-Jain, A., and Hurley, L. H. (2003) Two different chair-type G-quadruplex structures can form in the c-MYC silencer element and only one is stabilized by drugs, *Clin. Cancer Res. 9*, 6083S.
37. Seenisamy, J., Rezler, E. M., Powell, T. J., Tye, D., Gokhale, V., Joshi, C. S., Siddiqui-Jain, A., and Hurley, L. H. (2004) The dynamic character of the G-quadruplex element in the c-MYC promoter and modification by TMPyP4, *J. Am. Chem. Soc. 126*, 8702−8709.

38. Phan, A. T., Modi, Y. S., and Patel, D. J. (2004) Propeller-type parallel-stranded G-quadruplexes in the human c-myc promoter, *J. Am. Chem. Soc. 126*, 8710−6.
39. Phan, A. T., and Patel, D. J. (2003) Two-repeat human telomeric d(TAGGGTTAGGGT) sequence forms interconverting parallel and antiparallel G-quadruplexes in solution: Distinct topologies, thermodynamic properties, and folding/unfolding kinetics, *J. Am. Chem. Soc. 125*, 15021−7.
40. Grand, C. L., Han, H., Munoz, R. M., Weitman, S., Von Hoff, D. D., Hurley, L. H., and Bearss, D. J. (2002) The cationic porphyrin TMPyP4 down-regulates c-MYC and human telomerase reverse transcriptase expression and inhibits tumor growth in vivo, *Mol. Cancer Ther. 1*, 565−73.

BI0478190